AIP | Review of Scientific Instruments

Development of a new direct liquid injection system for nanoparticle deposition by chemical vapor deposition using nanoparticle solutions

Mattias Vervaele, Bert De Roo, Olivier Deschaume, Markku Rajala, Herve Guillon, Marilyne Sousa, Carmen Bartic, Chris Van Haesendonck, Jin Won Seo, and Jean-Pierre Locquet

Citation: Review of Scientific Instruments **87**, 025101 (2016); doi: 10.1063/1.4940937
View online: http://dx.doi.org/10.1063/1.4940937
View Table of Contents: http://scitation.aip.org/content/aip/journal/rsi/87/2?ver=pdfcov
Published by the AIP Publishing

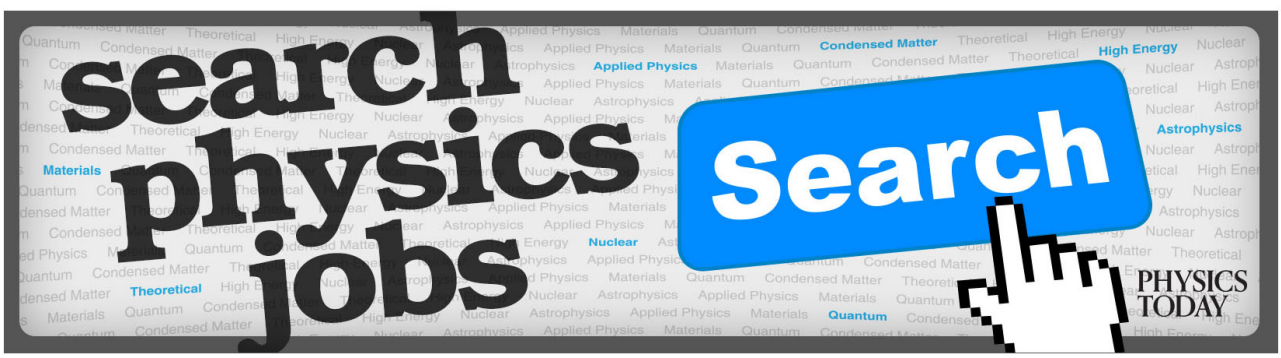

Development of a new direct liquid injection system for nanoparticle deposition by chemical vapor deposition using nanoparticle solutions

Mattias Vervaele,[1,a)] Bert De Roo,[1] Olivier Deschaume,[1] Markku Rajala,[2] Herve Guillon,[3] Marilyne Sousa,[4] Carmen Bartic,[1] Chris Van Haesendonck,[1] Jin Won Seo,[5] and Jean-Pierre Locquet[1]

[1]*Department of Physics and Astronomy, KU Leuven, BE-3001 Leuven, Belgium*
[2]*DCA Instruments, 20360 Turku, Finland*
[3]*Kemstream, 34055 Montpellier, France*
[4]*IBM Research, 8803 Rüschlikon, Switzerland*
[5]*Department of Materials Engineering, KU Leuven, BE-3001 Leuven, Belgium*

(Received 15 October 2015; accepted 16 January 2016; published online 4 February 2016)

Nanoparticles of different materials are already in use for many applications. In some applications, these nanoparticles need to be deposited on a substrate in a fast and reproducible way. We have developed a new direct liquid injection system for nanoparticle deposition by chemical vapor deposition using a liquid nanoparticle precursor. The system was designed to deposit nanoparticles in a controlled and reproducible way by using two direct liquid injectors to deliver nanoparticles to the system. The nanoparticle solution is first evaporated and then the nanoparticles flow onto a substrate inside the vacuum chamber. To allow injection and evaporation of the liquid, a direct liquid injection and vaporization system are mounted on top of the process chamber. The deposition of the nanoparticles is controlled by parameters such as deposition temperature, partial pressure of the gases, and flow rate of the nanoparticle suspension. The concentration of the deposited nanoparticles can be varied simply by changing the flow rate and deposition time. We demonstrate the capabilities of this system using gold nanoparticles. The selected suspension flow rates were varied between 0.25 and 1 g/min. AFM analysis of the deposited samples showed that the aggregation of gold nanoparticles is well controlled by the flow and deposition parameters. © *2016 AIP Publishing LLC.* [http://dx.doi.org/10.1063/1.4940937]

I. INTRODUCTION

Thin films containing nanoparticles (NPs) are expected to offer efficient and flexible tools for applications in a variety of industries such as electronics, catalysis, and sensors. Interest arises from the wide range of functionalities that the films can display including optical, catalytic, electrical, and thermal functionalities;[1–4] all largely determined by the composition, size, morphology, and surface properties of the NPs forming the film. NPs can have very different properties with respect to their relative bulk composition due to quantum confinement or large surface/volume ratio. A large body of research is focusing on the development and optimization of NP synthesis routes to control the size, shape, and surface charge of the final material. However, less effort is devoted to the incorporation of these NPs into thin films.

Currently, different approaches exist to produce NP thin films. The most promising methods are chemical vapor deposition (CVD) and magnetron sputtering, although other methods such as laser ablation, electrodeposition, ion beam deposition, and ion beam implantation are also used.[5–7] In most of them, the NPs are formed *in situ* or concurrently with the matrix, for instance, through annealing of deposited layers or implanted species. This significantly limits the type of NP that can be incorporated. The use of preformed NPs—for instance, through chemical methods—is highly desirable as a much wider range of materials and shapes can be included. When the deposition and the NP formation steps are separated, both can be individually optimized. This can be a crucial advantage for more complex nano-shapes and structures. The deposition of preformed NPs has recently become possible with CVD,[8] in which a novel methodology is based on the incorporation of an aerosol to allow for the transport of the preformed NPs. These may be incorporated into a conventional CVD flow (hybrid CVD) or transported with another semiconductor precursor (aerosol assisted CVD or AACVD).[9] These techniques have several benefits: first of all, their flexibility. Many preformed NP solutions can be used to produce different types of nanocomposite films. Changing the content of the precursor reservoir can control film doping, and the precursor solution containing the preformed NPs can be deposited along with any chemically compatible precursor to produce a wide range of nanocomposite thin films.[8,10–12] Second, the attractivity of CVD due to the control it offers over film composition, coverage, and uniformity. Third, their wide use in industrial applications such as microelectronics and glazing. Finally, the techniques are relatively simple one step processes that do not require aging times or special handling steps.[3,8] Within CVD processing, there is a growing tendency to use liquid precursors instead of gases. Their popularity can be explained by their lower toxicity, flammability, or reactivity with respect to gaseous ones.[13] While new direct liquid injection (DLI) evaporation technologies have solved some former problems

a)Electronic mail: mattias.vervaele@fys.kuleuven.be

related to the vaporization of precursors such as not allowing stable and reproducible vapor flows, our NP injector head improves on this technology. It has many advantages including preventing undesirable and premature thermal decomposition and preventing vaporizer clogging. Also, the NP injector is able to handle and vaporize most solid and liquid organic, organometallic, or inorganic compounds including low vapor pressure, thermally labile, and viscous ones.[14] Moreover, the NP injector is mounted on top of the process chamber, where the latter is able to work under vacuum conditions enabling easier control of the deposition parameters.

In most applications, a good control over the properties of NPs is desired. The targeted physical properties depend strongly on parameters such as the morphology, polydispersity, and crystallinity of the NPs. Using wet chemistry methods, one can get a good control of these parameters. In this study, gold NPs (GNPs) are used as a model system as they are well studied and their synthesis is relatively simple.[15] Moreover, they have been studied extensively due to their unique optical properties, mainly in the visible spectral range.[16] They are typically used as catalysts for the growth of nanowires made of a wide range of materials such as ZnO, Si, and Ge as well as the active sites for surface enhanced Raman scattering (SERS) applications.[17–19] The experimental setup used and described below is a novel nanoparticle vapor deposition (NVD) system designed and manufactured by DCA Instruments combined with a DLI Vapbox 1500 NP injector (Kemstream).

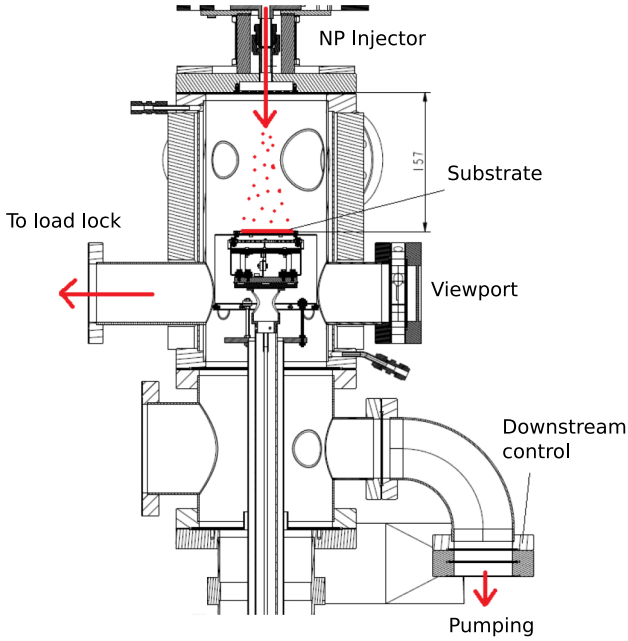

FIG. 1. A schematic of the process chamber.

II. INSTRUMENTS

A. Vacuum system

The NVD system that was used for the deposition of the NP thin films was designed and manufactured by DCA Instruments. The vacuum system consists of a load lock and a process chamber, which are separated by a gate valve. The load lock allows substrate loading without venting the process chamber. The load lock is equipped with both convectron and ion gauges for pressure monitoring. It is evacuated by a turbo pump with a scroll pump as backing pump. The process chamber pumping is done via a dry pump (ixH100 Edwards), which is capable of pumping very high gas loads during the process. For a precise downstream control of the process pressure, a butterfly valve is mounted between the dry pump and the process chamber. The process chamber is equipped with convectron and Baratron gauges, and the latter is used for accurate downstream control together with the butterfly valve. A schematic of the process chamber and the operation principle can be seen in Figures 1 and 2, respectively. The

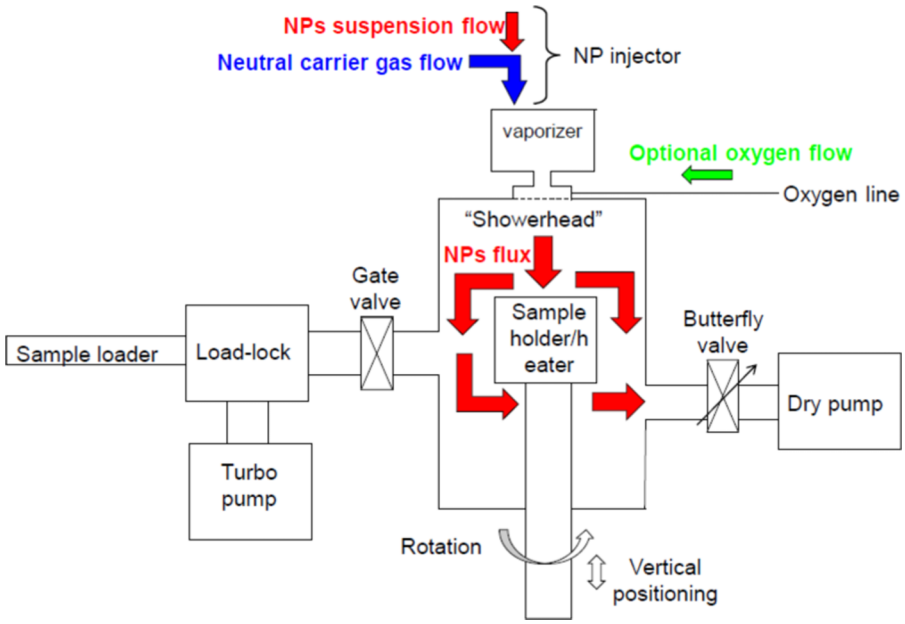

FIG. 2. Vacuum system with the NP injector integrated.

sample manipulator can handle substrate sizes of 2 in. Heating of the substrate is possible up to 1000 °C and rotation up to 60 RPM. The distance between the substrate level and NP injector outlet can be varied between 157 mm and 257 mm.

B. NP injector

The Vapbox 1500 (Kemstream) possesses two injector heads that can be operated simultaneously. This is advantageous when the co-deposition of NPs and a matrix is wanted. A schematic of the Kemstream injection head is shown in Figure 3. The liquid is mixed with a carrier gas to obtain an aerosol. The contents of this aerosol can be optimized by changing the injection frequency and the liquid flow. The flow of the NPs precursor is monitored with a liquid mass flow meter and the flow of the gas is monitored with a gas mass flow meter. The carrier gas flow can be varied between 150 and 2000 SCCM and the liquid flow between 0.1 and 3 g/min. The aerosol is then injected into a 1500 cm^3 heated stainless steel atomization/flash vaporization chamber. This vaporization chamber has three heated zones (zone 1: top plate of the vaporizer inside which the injection heads are plugged, zone 2: vaporizer body, and zone 3: bottom plate of the vaporizer where the vapors exhaust is located) to ensure a homogeneous temperature in the chamber and the total vaporization of the solvents. Heating of the three independent zones is possible up to 300 °C. The gas with the NPs can then flow into the process chamber. The Vapbox 1500 is mounted on top of the process chamber.

One of the main advantages of using this injection system is the possibility of loading the precursors into the vessels in advance, which allows to inject NPs into the process chamber without having to rely on chemical reactions *in situ*, as it is usually common. The density of the NPs can be modified by adjusting the parameters of the deposition such as injection flow rate and deposition time. Figure 4 is a scheme of the injector with all its accessories, i.e., a liquid panel with one liquid flow meter per injection head, a carrier gas panel with one carrier gas mass flow meter per injection head, an ICU (Injection Control Unit), and a TCU (Temperature Control Unit).

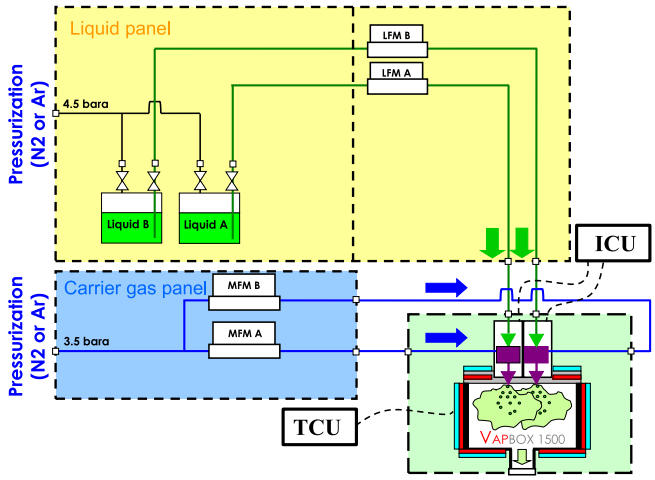

FIG. 4. Scheme of the Vapbox 1500 NP injector and its accessories.

C. Characterization instruments

1. Transmission electron microscopy

TEM measurements were performed with a transmission electron microscope (CM 200 FEG Philips) operating at 200 keV. The TEM samples were prepared by placing 8–10 μl of particle solution on a carbon-coated copper grid and dried under ambient conditions. At least 100 particles were analyzed to determine the mean radius and standard deviation. Those were analyzed with ImageJ[20] and the psa-macro (The macro is available at http://www.code.google.com/p/psa-macro).

2. Atomic force microscopy

An Agilent 5500 AFM system with MSNL-F cantilevers (f = 110–120 kHz, k = 0.6 N/m) with average tip radius of 2–12 nm was used for the morphological imaging. The AFM topography images were leveled, line-corrected, and measured (height profiles and histograms) using Gwyddion,[21] a free and open-source SPM (scanning probe microscopy) data visualization and analysis program.

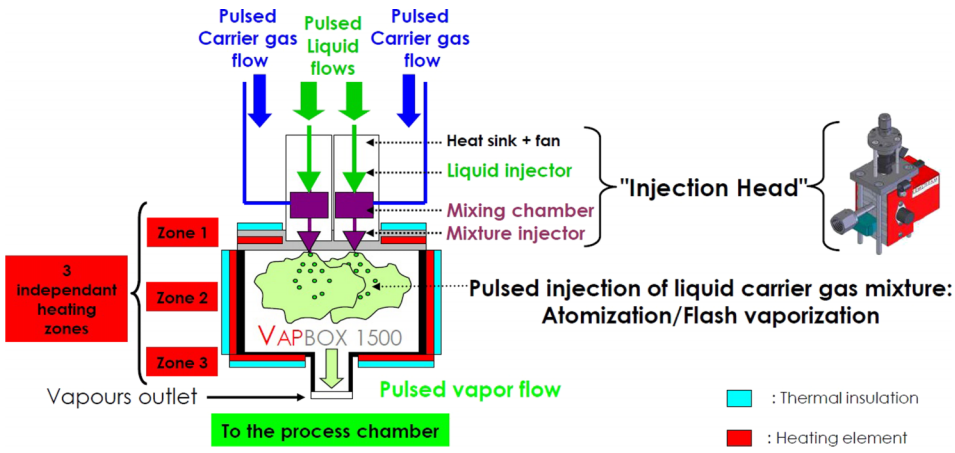

FIG. 3. A schematic of the Kemstream Vapbox 1500 injection head.

III. EXPERIMENTAL METHODS

A. Chemicals

All chemicals (cetyltrimethylammonium bromide (Sigma-Aldrich, 99%), gold(III) chloride trihydrate (Sigma-Aldrich, ≥99.9% trace metals basis), water (MilliQ, 18 MΩ), toluene (Acros, 99.85%), cyclohexane (Acros, 99.5%), and dodecanethiol (Sigma-Aldrich, ≥98%)) were used as received without further purification. The GNPs were synthesized using two-phase reduction of $AuCl_4$, following the procedure of Brust *et al.*,[22] resulting in NPs of ca. 3 nm diameter. First, aqueous hydrogen tetrachloroaurate (30 ml, 30 mM) was mixed with tetraoctylammonium bromide in toluene (80 ml, 50 mM) and vigorously stirred until all the tetrachloroaurate was transferred into the organic layer. Second, dodecanethiol (170 mg) was added to the organic phase. A solution of sodium borohydride was added dropwise under vigorous stirring. After 3 h stirring, the organic phase was separated, evaporated to 10 ml in a rotary evaporator, and mixed with 400 ml ethanol to remove excess thiol. The mixture was kept for 4 h at −18 °C and the dark brown precipitate was filtered off and washed with ethanol. The crude product was dissolved in 10 ml toluene and again precipitated with 400 ml ethanol. The result was a black precipitate, which was redissolved in cyclohexane. The particles seemed not to degrade over time, which was controlled by TEM measurements 4 weeks after preparation.

B. Measurements

To demonstrate the capabilities of the system, gold NPs were deposited on a silicon substrate. The different parameters of the experiments carried out in the deposition chamber are given in Table I. In every case, the temperature in the three zones of the vaporizer was the same; therefore, it is simplified to only one value. The changed variables were the flow rate (1 g/min and 0.25 g/min), vaporizer temperature (115 °C and 100 °C), and duration of the deposition (10 min and 80 min). The rest of the parameters were the same in all the experiments. The NPs' concentration used was 30 mg/300 ml cyclohexane and anhydrous nitrogen as carrier gas. The wafer was heated to 150 °C. The pressure in the liquid line and carrier gas line was 3.5 bars and 2.5 bars, respectively. The carrier gas flow was 500 SCCM and the distance between the substrate and shower head was 247 mm.

TABLE I. List of the parameters used in the deposition tests.

Nanoparticles	GNP
Solvent	Cyclohexane
Carrier gas	Anhydrous nitrogen
NPs concentration in suspension	30 mg/300 ml
Suspension flow rate	1 g/min or 0.25 g/min
P liquid line	3.5 bars
Carrier gas flow	500 SCCM
P carrier gas line	2.5 bars
Vaporizer temperature	115 °C or 100 °C
Substrate temperature	150 °C
Duration of process	10 min or 80 min
Distance substrate and shower head	247 mm

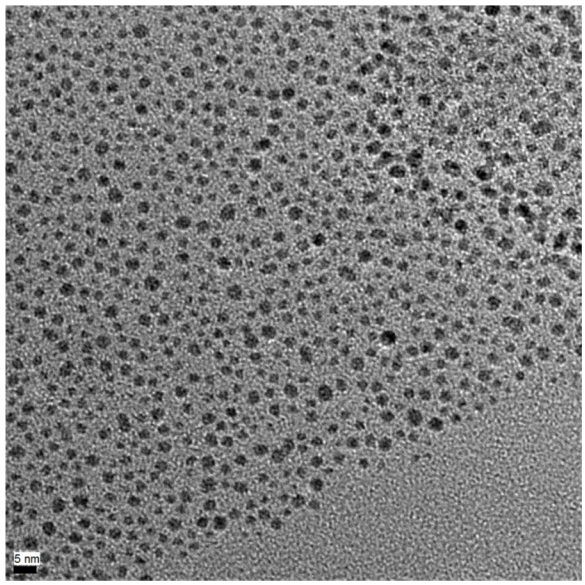

FIG. 5. TEM image of the synthesized GNPs onto a grid with a scale bar of 5 nm.

IV. EXPERIMENTAL RESULTS

In Figure 5, a TEM image of the synthesized GNPs before deposition following the Brust method[22] is shown. The average diameter of the GNPs was 2 nm with a standard deviation of 0.6 nm. The size distribution of the NPs is given in Figure 6.

A. High flow rate

In the first set of experiments, a flow rate of 1 g/min for 10 min and a vaporization temperature of 115 °C were used. This led to the accumulation of GNPs in a spot of around 1 cm diameter, as illustrated in the AFM pictures of Figure 7. The accumulation is clearly visible in the middle of the spot, whereas more distinct GNPs of a few nm diameter were visible at the edge. Nanodroplets might be formed in the plume from the gas phase. The formation of either nanocrystals, and/or

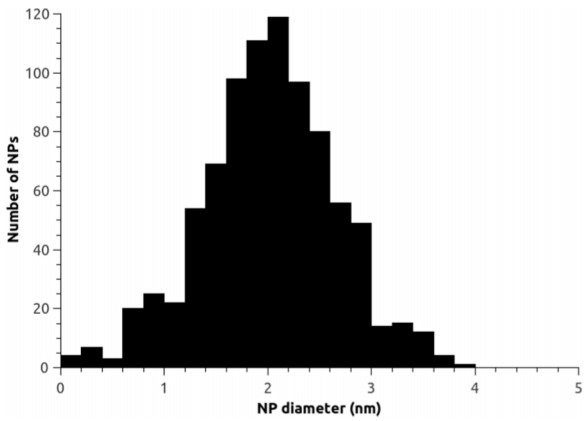

FIG. 6. Size distribution of the synthesized GNPs.

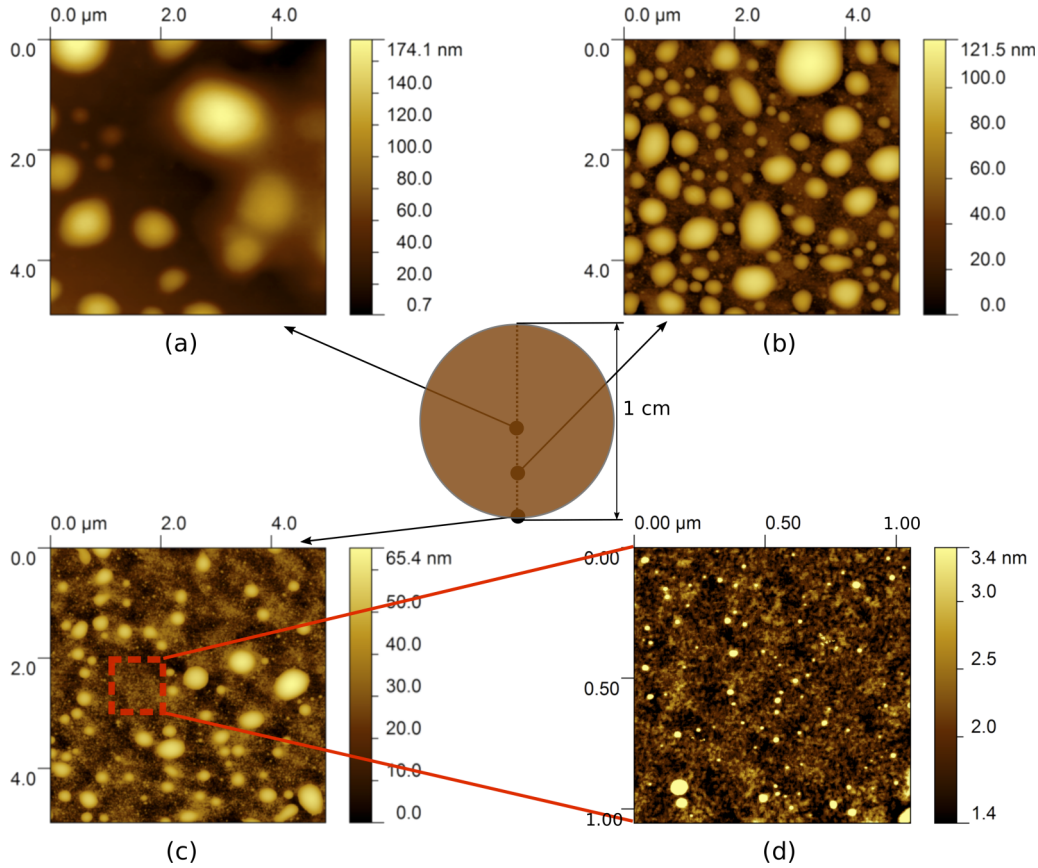

FIG. 7. AFM image of the sample with a suspension flow rate of 1 g/min taken at different positions across the NP covered area. A scanning area of 5 μm×5 μm (a) in the middle of the spot, (b) halfway between middle and edge of the spot, and (c) at the edge of the spot. (d) Zoom in of a region in (c) on a scanning area of 1 μm×1 μm. In the middle of the spot, accumulation of GNPs to microstructures is found, whereas more distinct GNPs are found at the edge.

liquid hot droplets, solidification, or agglomeration in the plume is governed by the thermodynamic conditions (pressure and temperature) and the density during the nucleation time of the droplets.[23] Optimization of experimental configurations, such as variation of flow rate and vaporization temperature, has been applied to reduce the formation of micro-droplets.

B. Low flow rate

In the second set of experiments, the flow rate has been changed to 0.25 g/min for 80 min and a vaporization temperature of 100 °C. Figure 8 shows an AFM image of this sample measured at two different points (a) and (b). These points were chosen near the center of the wafer, because no clear spot was seen in the case with the lower flow rate. As compared to the sample prepared with a higher flow rate, the distribution of GNPs is much more homogeneous. The height of the NPs clusters is smaller and the dispersion is smaller. Although the total amount of NP solution deposited is double in the case of the lower flow rate (20 g vs. 10 g), the limited AFM measurement area, the accumulation of NPs at higher flow rate, and the potentially incomplete vaporization process, we cannot easily compare the total amount of NPs deposited in the two cases. Nevertheless, a high flow rate (1 g/min) is clearly not the best option for obtaining a uniform layer of GNPs, and therefore, a longer deposition time at a

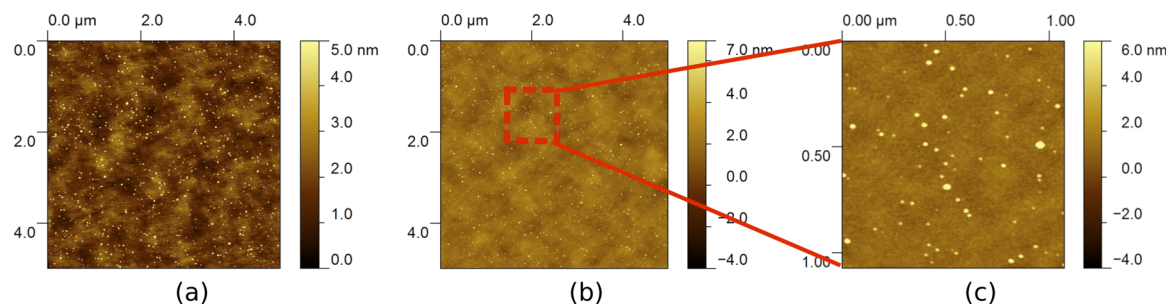

FIG. 8. AFM image of sample with a suspension flow rate of 0.25 g/min at two different spots (a) and (b) with a scanning area of 5 μm×5 μm. (c) Zoom in of a region in (b) on a scanning area of 1 μm×1 μm.

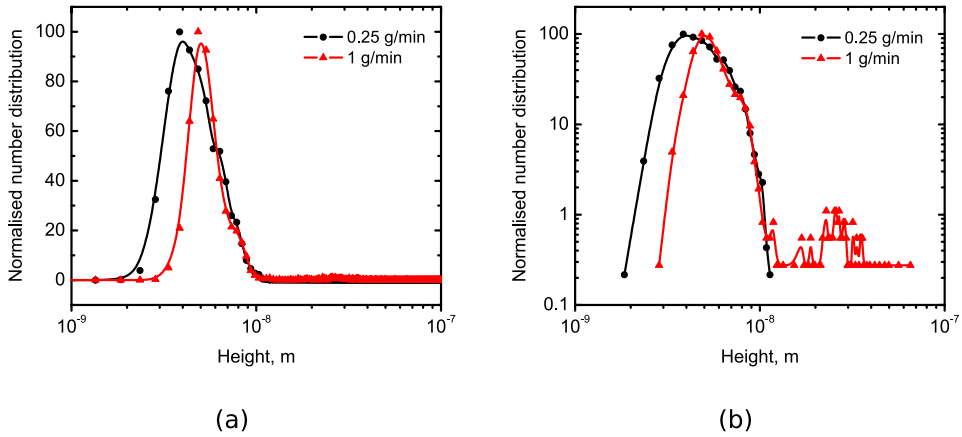

FIG. 9. NP height number distributions. (Left) On a semi-log scale and (right) on a log-log scale to show the number of large aggregates.

smaller flow rate is more favorable for a homogeneous NP deposition.

The NP height number distribution obtained from the different AFM pictures can be seen in Figure 9. The average diameter found for the sample with 0.25 g/min is 5.23 nm with a standard deviation of 1.05 nm. The higher value compared with the TEM measurements can be explained by the fact that the GNPs are stabilized with dodecanethiol, which can be seen with AFM and not with TEM. At higher flow, the particles coalesce and the main particle size distribution shifts to larger sizes.

Figure 10 is an AFM image of the sample with flow rate of 0.25 g/min with scale bar closer to the NPs, in order to be able to compare NP sizes before and after the deposition. The height is within the expected range, while the lateral resolution is lower; the NPs are seen at least 7–10 nm bigger due to tip convolution effects. Therefore, average NP height is chosen as average diameter in order to avoid tip convolution effects. Moreover, the particles height may be expected to be ~3.6 nm higher than estimates of diameter obtained from TEM characterization owing to the presence of the dodecanethiol layer and specific tip-particles interactions due to the presence of the hydrophobic coating.

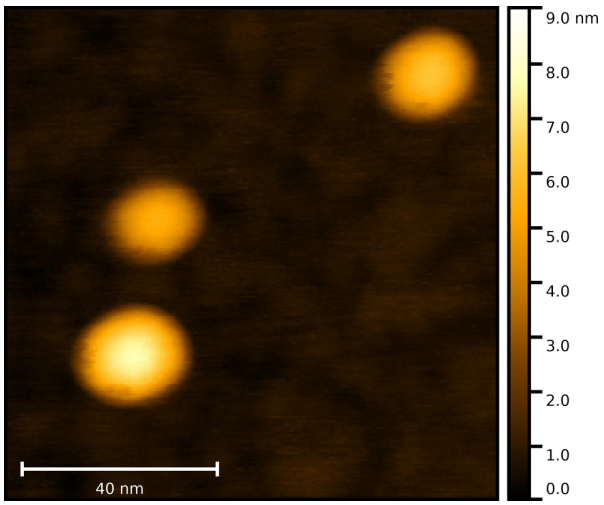

FIG. 10. Zoom in on sample with 0.25 g/min deposition rate. The height is within the expected range, while the lateral resolution is lower due to tip convolution effects.

V. CONCLUSION

We have developed a new system for the deposition of NPs by nanoparticle vapor deposition. The direct liquid injection system Vapbox 1500 by Kemstream was mounted on top of the process chamber and allowed the injection of liquid and gas. The concentration of the deposited NPs could be varied simply by changing the liquid flow rate. The performance of the system was studied under two different operating conditions. GNPs were used as model metal NPs and the selected flow rates varied between 1 g/min and 0.25 g/min. AFM analysis of the deposited samples showed that the size of the GNPs deposited with a lower flow of 0.25 g/min matches that measured with TEM before injection. This shows that it can be used to further develop thin film applications based on NPs technology and properties. A big advantage of this technique is the wide range of films that can be produced by varying the precursors and NPs used. Perhaps more important is the general applicability; CVD is already widely used in the glazing and microelectronics industries; hence, this approach could be easily integrated into the design of useful products and devices.

ACKNOWLEDGMENTS

We thank the EU for supporting via the FP-7 grant SNOWCONTROL project (No. 263510). B.D.R. acknowledges financial support from the Agency for Innovation by Science and Technology in Flanders (No. IWT/121661). C.B. and C.V.H. acknowledge financial support from the Hercules Foundation (Project No. HER/09/021). J.W.S. acknowledges financial support from the Hercules Foundation (Project No. HER/08/25). We thank Jean Fompeyrine for his expertise on thin film deposition processes and safety as well as Stijn Vandezande and Bastiaan Opperdoes for their considerable technical support.

[1]P. K. Jain, X. Huang, I. H. El-Sayed, and M. A. El-Sayed, Plasmonics **2**, 107 (2007).
[2]G. Walters and I. P. Parkin, J. Mater. Chem. **19**, 574 (2009).
[3]P. Marchand, I. A. Hassan, I. P. Parkin, and C. J. Carmalt, *Dalton Transactions* (Cambridge, England, 2003), Vol. 42, p. 9406.
[4]G. V. Ramesh, S. Porel, and T. P. Radhakrishnan, Chem. Soc. Rev. **38**, 2646 (2009).
[5]K. Lukaszkowicz, in *Review of Nanocomposite Thin Films and Coatings Deposited by PVD and CVD Technology*, edited by M. M. Rahman (InTech, 2011).

[6]N. A. Sam Zhang, in *Nanocomposite Thin Films and Coatings, Processing, Properties and Performance*, edited by N. A. Sam Zhang (Imperial College Press, 2007).
[7]M. Roy, in *Surface Engineering for Enhanced Performance Against Wear*, edited by M. Roy (Springer, 2013).
[8]R. G. Palgrave and I. P. Parkin, J. Am. Chem. Soc. **128**, 1587 (2006).
[9]X. Hou and K.-L. Choy, Chem. Vap. Deposition **12**, 583 (2006).
[10]C. R. Crick, J. C. Bear, P. Southern, and I. P. Parkin, J. Mater. Chem. A **1**, 4336 (2013).
[11]L. Avril, J. Boudon, M. M. de Lucas, and L. Imhoff, Vacuum **107**, 259 (2014).
[12]L. Avril, S. Bourgeois, M. M. de Lucas, B. Domenichini, P. Simon, F. Addou, J. Boudon, V. Potin, and L. Imhoff, in *13th European Vacuum Conference Joint meeting with 7th European Topical Conference on Hard Coatings and 9th Iberian Vacuum Meeting* [Vacuum **122**(Part B), 314 (2015)].
[13]H. Boer, Journal de Physique IV **5**, C5–961 (1995).
[14]H. Guillon and S. Bonnafous, Gases & Instrumentation Magazine (May-June 2008), pp 17-19.
[15]M.-C. Daniel and D. Astruc, Chem. Rev. **104**, 293 (2004).
[16]S. Link, S., and M. A. El-Sayed, J. Phys. Chem. B **103**, 8410 (1999).
[17]P. Kratzer, S. Sakong, and V. Pankoke, Nano Lett. **12**, 943 (2012).
[18]Y. Homma, Catalysts **4**, 38 (2014).
[19]Y. Zhang, W. Chu, A. D. Foroushani, H. Wang, D. Li, J. Liu, C. J. Barrow, X. Wang, and W. Yang, Materials **7**, 5169 (2014).
[20]M. D. Abràmoff, P. J. Magalhães, and S. J. Ram, Biophotonics Int. **11**(7), 36 (2004).
[21]D. Necas and P. Klapetek, Cent. Eur. J. Phys. **10**, 181 (2012).
[22]M. Brust, M. Walker, D. Bethell, D. J. Schiffrin, and R. Whyman, J. Chem. Soc., Chem. Commun. **7**, 801 (1994).
[23]A. C. Cefalas, S. Kobe, E. Sarantopoulou, Z. Samardzija, M. Janeva, G. Drazic, and Z. Kollia, Phys. Status Solidi A **205**, 1465 (2008).